ORIGINAL PAPER

Petrologically controlled oxygen isotopic classification of cogenetic magmatic and metamorphic sapphire from Quaternary volcanic fields in the Eifel, Germany

Sebastian Schmidt[1] · Andreas Hertwig[1,3] · Katharina Cionoiu[1] · Christof Schäfer[2] · Axel K. Schmitt[1,3]

Abstract

Gem sapphire is commonly retrieved from primary and secondary deposits associated with alkali basaltic fields, but its source rocks are rarely preserved. The Eifel (Rhenish Massif, western Germany), although not producing gem sapphire, shares many petrologic and geochemical similarities with such fields worldwide. Due to the young age of volcanic deposits and active quarrying, sapphire-bearing rocks are readily accessible, along with detrital sapphire from modern sediments. Here, oxygen isotope and trace element compositions are reported for 223 sapphire grains, and rutile and zircon inclusions in sapphire were dated indicating crystallization synchronous with Paleogene–Quaternary volcanism. Endmembers in $\delta^{18}O$ range are sapphires from syenites representing mantle-derived differentiated melts with minor crustal contamination (~4–6‰) and contact metamorphic mica schists (>10‰) as purely crustal source rocks. Intermediate values between ~6 and 10‰ require variable degrees of mantle-crust hybridization. Lower crustal granulite sources are dismissed based on their oxygen isotopic compositions being lower than most sapphire crystals. Diffusion modelling of sharp oxygen isotopic zonation in compositionally zoned crystals precludes crystal residence at >900 °C over the lifetime of evolved magma reservoirs in the Eifel (c. 50 ka). This argues against direct mantle or lower crustal sapphire origins. Instead, low temperature residence is consistent with sharp $\delta^{18}O$ gradients, coexisting andalusite, and fluid inclusion barometry. Hence, Eifel sapphire crystallization is attributed to contact metamorphic aureoles around upper crustal (5–7 km) magma bodies where phonolite, trachyte, and carbonatite melts differentiated from mafic parental magmas, and reacted with metasedimentary wall rocks.

Keywords Corundum · Intraplate volcanism · Alkaline magmatism · Contact metamorphism · Secondary ionization mass spectrometry

Introduction

Corundum with its diverse color varieties, primarily sapphire (blue, yellow, and green; BYG) and ruby (pink), ranks atop in price per carat for colored gemstones (Giuliani and Groat 2019). Gem sapphire is often found in intraplate volcanic fields dominated by alkaline mafic magmas, either in primary or secondary occurrences (Giuliani et al. 2014; Simonet et al. 2008), but the exact relationship between sapphire and its volcanic host rocks often remains ambiguous. Proposed mechanisms to explain the common yet enigmatic association between sapphire and alkaline magmas in intraplate settings include accidental sampling of xenocrysts from Al-enriched metasediments (e.g., Levinson and Cook 1994; Wörner et al. 1982), crystallization in various magmas including syenites and carbonatites at mantle or crustal depths (e.g., Baldwin et al. 2017; Sutherland et al. 1998), or formation in granitoid rocks or magma hybridized with Si-deficient silicate or carbonatite melts (Guo et al. 1996) from which sapphire is scavenged by transient mafic magma pulses. Identifying suitable properties to pinpoint the geologic and by proxy geographic origin of gem corundum becomes increasingly important for supply chain traceability

(e.g., Stone-Sundberg et al. 2017; Stone-Sundberg et al. 2021). Trace element abundances in natural corundum (mainly Mg, Ti, V, Cr, Fe, and Ga) have been evaluated as genetic indicators (Groat et al. 2019; Simonet et al. 2008), whereas trace Be enrichment above natural levels is indicative for heat-induced color enhancement allowing detection of undisclosed treatment (Emmett et al. 2003). However, the nearly pure Al_2O_3-chemistry of corundum challenges the applicability of trace element fingerprinting, and existing genetic classification schemes (e.g., Peucat et al. 2007) can be ambiguous when applied to locations beyond those from which the original training data for discrimination schemes were obtained (e.g., Palke et al. 2017). As an alternative, O-isotopic variability in corundum has been successfully harnessed to identify petrological processes and tectonic settings of corundum formation (e.g., Wong and Verdel 2018, and references therein). Early O-isotope studies of corundum employed the laser-fluorination technique requiring mg-sized powder aliquants (e.g., Giuliani et al. 2009), but more recently, secondary ionization mass spectrometry (SIMS) has moved to the foreground because it affords faster analysis and higher throughput. Moreover, SIMS is spatially selective at a minimal sample consumption of <1 ng, thus permitting the reconstruction of changes in the crystallization environment as recorded in isotopically zoned crystals (e.g., Palke et al. 2017; Sutherland et al. 2017; Turnier et al. 2020; Sorokina et al. 2021).

Here, we performed SIMS analysis of O-isotopes in natural corundum from the Eifel (Germany, Fig. 1), specifically the BYG sapphire varieties, to discriminate between formation processes in an intraplate volcanic setting. Although economically exploitable gem-grade sapphire has not been identified in the Eifel, its geodynamic setting as part of the Cenozoic Central European Volcanic Province (e.g., Wilson and Downes 2006) is nonetheless typical for global sapphire gem occurrences, which include intraplate basaltic volcanic fields and associated placer deposits in the Massif Central (France; Giuliani et al. 2009), Ankaratra and Antsiranana (Madagascar; Giuliani et al. 2007; Rakotosamizanany et al. 2014), as well as occurrences in eastern China, Southeast Asia, and eastern Australia (e.g., Guo et al. 1996; Sutherland et al. 2015, 2009a, 2009b). In contrast to previous studies, the Eifel stands out by its young age with the voluminous eruption of Laacher See volcano having occurred only c. 13 ka ago (Reinig et al. 2021). Sapphire-bearing lithic ejecta clasts are sometimes found in pyroclastic deposits from Eifel volcanoes, thus preserving a petrologic context for interpreting its O-isotope composition. Moreover, rapid SIMS analysis permits much more representative sampling of sapphire compared to previous studies (e.g., 25 grains in Giuliani et al. 2009, vs. 223 grains studied here). Based on O-isotopes, trace element data, and reconnaissance ages of rutile and zircon inclusions in sapphire, a close association

of magmatic, hybrid, and metamorphic types is documented for Eifel sapphire with near-mantle (~4–6‰), intermediate (~6–10‰), and elevated $\delta^{18}O$ compositions (~10–19‰), respectively. The presence of distinct genetic types of sapphire in close temporal and spatial association points to highly evolved syenitic intrusive margins of mid-upper crustal magma reservoirs and their contact metamorphic aureoles as incubators for sapphire in intraplate volcanic fields.

Intraplate magmatism and sapphire bearing xenoliths in the Eifel

The Eifel is a volcanic region in western Germany delineated by the Rhine river in the east, and together with the transrhenane Siebengebirge and Westerwald volcanic fields, it forms the westernmost extent of Cenozoic volcanism in the Rhenish Massif. It is part of the intra-continental Cenozoic Central European Volcanic Province (Fig. 1), which evolved contemporaneously with lithosphere-scale uplift of basement blocks and rift graben development since the Late Cretaceous. This province also includes the Massif Central, the Ohře (Eger) Graben, and Western Carpathian volcanic fields (Wilson and Downes 2006) for which sapphire has been previously described (e.g., Giuliani et al. 2009; Uher et al. 2012; Seifert et al. 2014). Volcanism in the Eifel started sporadically in the Cretaceous (Lippolt 1983) and intensified during the Paleogene (c. 44–39 Ma and 37–35 Ma; Fekiacova et al. 2007) Hocheifel volcanic phase. After a hiatus, it resumed during the Quaternary when two geographically separated subfields emerged along the southwestern and eastern flanks of the Hocheifel (Fig. 1): the West Eifel Volcanic Field (WEVF) and the East Eifel Volcanic Field (EEVF), respectively. The WEVF subfield has been intermittently active during the Quaternary from c. 600–11 ka and erupted dominantly mafic SiO_2-undersaturated nephelinites and sodic basanites in scoria cones and maars ($n \sim 240$; Schmincke 2007). By contrast, volcanism in the EEVF produced mainly voluminous phonolite-trachyte eruptions vented from the three episodically active volcanic complexes of Rieden, Wehr, and Laacher See between c. 460 and 13 ka (Van den Bogaard et al. 1987; Reinig et al. 2021;). In addition, small-volume potassic mafic magmas including nephelinite, leucitite, basanite, and tephrite erupted in scoria cone clusters around Laacher See ($n \sim 80$; Schmincke 2007). Besides the evolved magmas erupted from the Rieden, Wehr, and Laacher See complexes (e.g., Wörner and Schmincke 1984; Wörner et al. 1988), the presence of highly evolved melts is also documented by syenitic-carbonatitic plutonic ejecta clasts which are most abundant in EEVF phonolite-trachyte complexes (e.g., Schmitt et al. 2010), but also occur in some WEVF scoria cones (e.g., Riley et al. 1996; Schmitt et al. 2023a). These differences in predominant magma
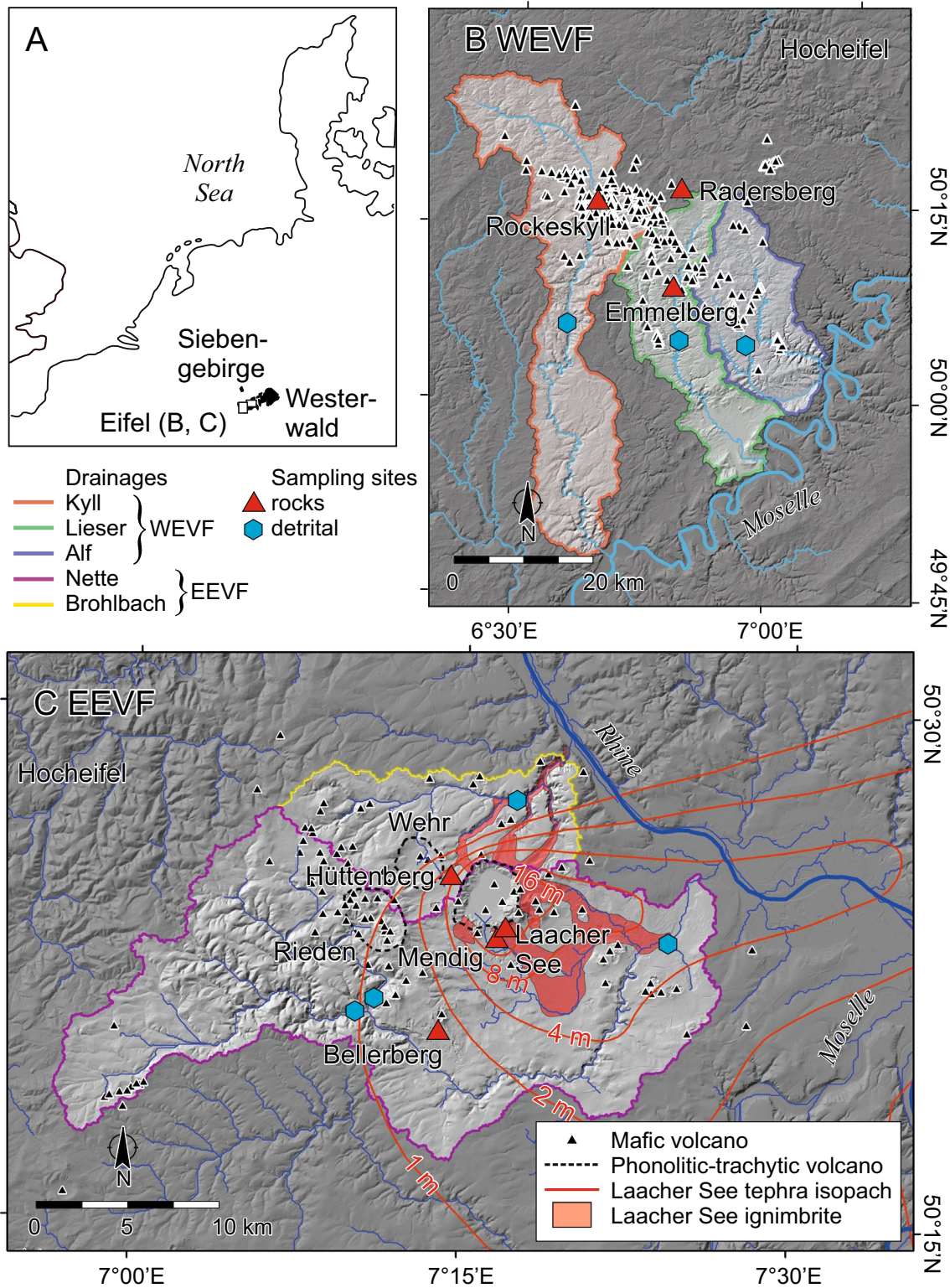
Fig. 1 Map of the study region showing the Paleogene–Quaternary volcanic fields of the Eifel, Siebengebirge, and Westerwald (**A**). Detailed maps of the West and East Eifel Volcanic Fields (**B** and **C** for WEVF and EEVF, respectively) adjacent to the Paleogene Hocheifel are shown with locations of scoria cones and maars (black triangles) and larger phonolitic/trachytic centers (dashed outlines). River drainage systems are marked along with sampling locations for lithic ejecta and sapphire-bearing lava as well as detrital samples. Digital elevation model is based on ASTER GTM2 data projected into UTM 32N, WGS84

compositions reflect different durations and depths for pre-eruptive magma storage. Mafic magmas in the WEVF ascended rapidly within few hours from mantle and lower crustal depths, whereas evolved magmas in the EEVF experienced protracted (c. 50 ka or more) residence in mid-upper crustal reservoirs (e.g., Berndt et al. 2001; Schmitt et al. 2010; Denis et al. 2013; Rout and Wörner 2020). Consistent with these different depths of magma origin, WEVF volcanoes frequently contain ultramafic xenoliths either derived from the mantle (e.g., Kempton et al. 1988; Shaw et al. 2005), or as cumulates from lower crustal magma reservoirs (e.g., Duda and Schmincke 1985; Schmitt et al. 2023a), whereas cogenetic syenites and low- to intermediate-grade metamorphic xenoliths from ~5 to 7 km depths are primarily associated with the evolved complexes of the EEVF (e.g., Wörner and Fricke 1984).

Sapphire crystals have been described from Eifel volcanic deposits as xenocrysts and in xenoliths (Grapes 1986; Hentschel 1987; Wörner and Fricke 1984; Wörner et al. 1982), and more recently (Schmitt et al. 2023b) as detrital grains in modern river sediment. The only detailed studies were on rare sapphire-bearing xenoliths found in the Hüttenberg Tephra of the Wehr volcanic complex, which show strong SiO_2 depletion relative to their pelitic protolith that Wörner et al. (1982) ascribed to partial melting and melt extraction of wall rock in the aureole of the Hüttenberg trachyte magma reservoir leaving behind an Al-rich restite. Grapes (1986) favored break-down of muscovite according to the reaction:

$$muscovite = corundum + peraluminous\ melt \qquad (1)$$
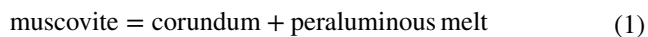
while biotite would simultaneously also react to produce peraluminous melt. Fluid inclusions in corundum from these xenoliths are CO_2-dominated and indicate entrapment at ~4–7 km depth and 600–700 °C (Wörner and Fricke 1984). This closely agrees with the storage depths of phonolite from Laacher See as constrained by volatiles in melt inclusions (Harms and Schmincke 2000) and experimental petrology (Berndt et al. 2001; Harms et al. 2004).

Analytical methods

Sample origins and preparation

Sapphire from the WEVF (Table 1) was extracted from cm-sized medium–coarsely crystalline lithic clasts from proximal scoria cone beds (Emmelberg: CSK-04, -16; Radersberg: CSK-17) and eroded deposits on fields east of the Rockeskyll composite scoria cone (CSK-12). For the EEVF (Table), sapphire was extracted from lithic clasts in scoria cones and associated lava flows (Bellerberg: CSK-30).

Trachytic pyroclastic deposits from the Wehr volcanic complex (Hüttenberg Tephra from the eponymous sand pit: CSK-06) and phonolite tephra from Laacher See volcano (Upper Laacher See Tephra at the location "In den Dellen": CSK-05) also contain rare sapphire-bearing ejecta clasts. One leucocratic xenolith was recovered from Mendig tephrite lava (CSK-13).

In addition to these primary sapphires (i.e. where petrographic context is preserved), secondary sapphire was collected as detrital grains in modern river sediments (Table 1). Based on a drainage basin analysis performed by using the ArcGIS Pro 2.9.3 "Watershed (Ready To Use)" tool, potential sampling sites in second order rivers in the area were identified (Fig. 1). The drainage basin analysis was overlain onto the geological map GÜK 300 (Landesamt für Geologie und Bergbau, Rheinland-Pfalz), and four locations each were sampled in the WEVF (Alfbach, Kleine Kyll, Kyll, and Lieser) and the EEVF (Brohlbach, Nette upstream, Nette downstream, and Nitzbach).

To extract sapphire from clasts, the rocks were gently crushed in a steel mortar. Due to the high frequency and size of the sapphire crystals, they were picked directly from the disintegrated rock. When the clasts were sufficiently large, polished petrographic thin sections were prepared (Fig. 2A, B), but clasts were generally too small for bulk geochemical analysis. For secondary sapphire extraction, ~1.5 kg of black sands rich in Fe-Ti oxides and other heavy minerals were concentrated on each site from the <5 mm sieve fraction by washing with a gold pan. Sapphire was then recovered from the black sand after cleaning with deionized water, drying in an oven at 50 °C for 48 h and sieving to a <500 μm grain size. Then, a magnetic separation was performed by using a Frantz magnetic separator LB-1 with a current of 0.8 A and a side slope of 20°. In a second step the separation was repeated with a current of 1.2 A and a side slope of 5°. Subsequently, the non-magnetic fraction was immersed in 80–85 wt.% aqueous lithium heteropolytungstate solution or diiodomethane, and the >2.9 g/cm^3 sink retained for hand-picking of sapphire (density 4.0 g/cm^3) that was identified by its blue color and morphology (Fig. 2C, D) by using a ZEISS Stemi 508 binocular microscope. All river sediment samples except that from Kleine Kyll yielded sapphire; for lack of difference, grains from the up- and downstream locations of the Nette river are treated together.

Seven 25.4 mm diameter epoxy sample mounts with 223 sapphire crystals total were prepared, five mounts with detrital ($n = 100$) and two with primary crystals ($n = 123$). Fragments of corundum reference material HD-LR1 (Schmidt et al. 2024) were placed in the center of the sample mounts and around the unknowns. The surfaces of the epoxy mounts were abraded and flattened with a diamond grinding wheel (MD-Piano, Struers). Subsequently, surfaces were polished with diamond suspension (DP-Suspension P, Struers) with

Table 1 Location and depositional context (subfield, host unit, and eruption age) of Eifel sapphire crystals

Location	Sample name	Subfield	Unit	Age (ka)	Latitude N	Longitude E	Petrological context	n	δ¹⁸O average	2 SD	δ¹⁸O minimum	δ¹⁸O maximum
Rockeskyll	CSK-12	WEVF	Rockeskyll scoria	470[1]	50°15.444'	6°40.684'	Mica schist	20	9.64	0.57	9.17	10.16
Emmelberg1	CSK-04	WEVF	Emmelberg scoria	48[2]	50°08.921'	6°48.415'	Syenite	20	4.81	0.40	4.50	5.34
Emmelberg2	CSK-16	WEVF	Emmelberg scoria	48[2]	50°08.921'	6°48.415'	Syenite	9	5.77	0.40	5.43	6.04
Radersberg	CSK-17	WEVF	Radersberg scoria	720–480[3]	50°16.430'	6°49.267'	Meta-psammite	15	10.80	0.54	10.29	11.44
Kyll	Kyll	WEVF	Sediment	Modern	50°05.979'	6°36.074'	Detrital	12	10.12	2.52	7.26	12.31
Lieser	Lieser	WEVF	Sediment	Modern	50°05.496'	6°49.099'	Detrital	5	8.30	3.08	5.96	9.59
Alfbach	Alfbach	WEVF	Sediment	Modern	50°04.798'	6°57.092'	Detrital	3	7.85	3.49	6.04	9.52
Bellerberg	CSK-30	EEVF	Bellerberg scoria	215–190[4]	50°21.126'	7°14.039'	Syenite	17	6.45	0.55	5.82	6.84
Hüttenberg	CSK-06	EEVF	Hüttenberg Tephra	215[5]	50°25.728'	7°13.866'	Hornfels	14	9.18	1.22	8.17	10.25
Laacher See	CSK-05	EEVF	Upper Laacher See Tephra	13[6]	50°24.344'	7°16.067'	Hornfels	14	7.83	0.48	7.24	8.26
Mendig	CSK-13	EEVF	Mendig lava	156[7]	50°23.329'	7°16.651'	Hornfels	14	7.89	0.43	7.46	8.22
Nette1	Ne1	EEVF	Sediment	Modern	50°23.301'	7°23.987'	Detrital	16	7.83	1.98	6.54	9.62
Nette2	Ne2	EEVF	Sediment	Modern	50°21.185'	7°10.913'	Detrital	Combined with Ne1				
Nitzbach	Ni	EEVF	Sediment	Modern	50°21.136'	7°09.963'	Detrital	5	8.34	3.67	6.29	11.03
Brohlbach	Br	EEVF	Sediment	Modern	50°27.357'	7°17.802'	Detrital	59	13.76	5.26	7.85	18.94

Petrological type (ejecta clast type, xenocryst host, or detrital) is stated along with summary of O-isotopic compositions (average, minimum, and maximum values)

Delta values in permil relative to V-SMOW ¹⁸O/¹⁶O = 0.0020052

(1) Shaw et al. (2010), (2) Sun and Schmitt (2019), (3) Mertz et al. (2015), (4) Van den Bogaard et al. (1987), (6) Reinig et al. (2021), (7)Wagner and Storzer (1970)

Fig. 2 Photomicrographs of thin sections (plane polarized light) with sapphire grains in situ from lithic ejecta with sample designations **A** CSK-05 (Laacher See Tephra) and **B** CSK-12 (Rockeskyll). Focus-stacked photomicrographs of detrital sapphire from Nette river sediments (**C**, **D**)
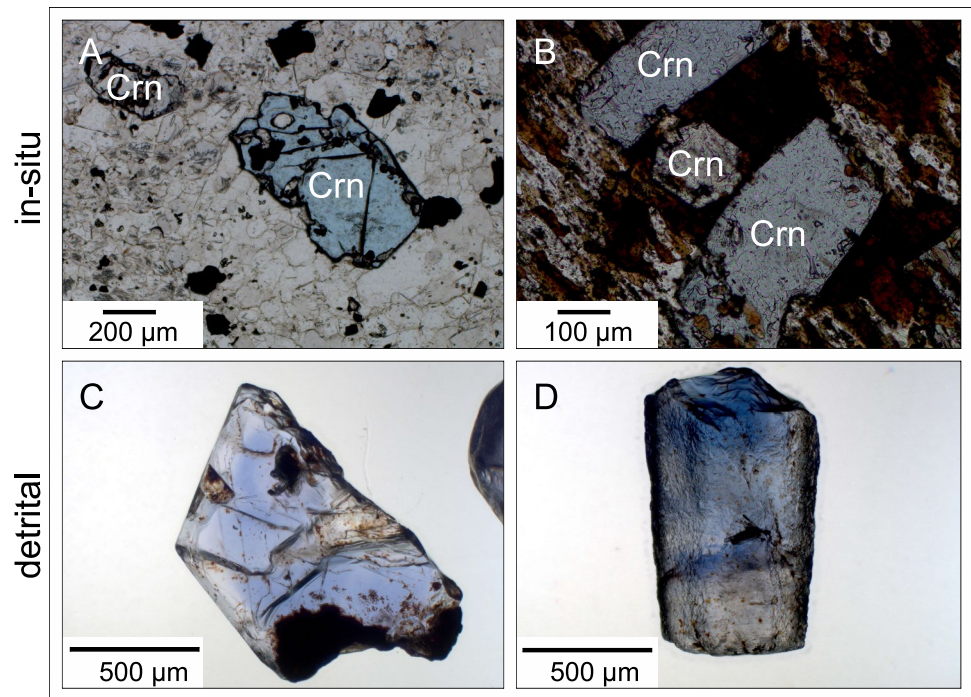
a progressively smaller grain size from 3 to 1 μm and an alcohol-based lubricating agent (DP-Lubricant Blue, Struers) on a rubber-like surface polishing wheel (MD-Largo, Struers). Mount surfaces were cleaned successively with ethylenediaminetetraacetic acid (EDTA) + ammonia (NH_3), purified water, and methanol using an ultrasonic bath, and then conductively coated with ~9 nm carbon and ~40 nm gold by using a QUORUM Q15OT ES coater for electron microbeam and SIMS analyses, respectively.

## Phase and compositional analysis

Scanning electron microscope, electron microprobe, and Raman microscope

Backscattered electron (BSE) images were taken with a ZEISS WITec RISE EVO MA15 SEM at the Institute of Earth Sciences, Heidelberg University to assess chemical homogeneity, to reliably distinguish sapphire from other mineral phases, and to detect the presence of inclusions (Fig. 3). An accelerating voltage of 18 kV and a probe current of 9 nA were used. Mineral inclusions were analyzed with an Oxford Instruments X-MaxN 150 mm^2 energy-dispersive X-ray spectrometry (EDS) detector. Trace element composition of Eifel sapphire were determined by using a JEOL JXAiSP100 electron probe microanalyzer (EPMA) equipped with five wavelength dispersive spectroscopy (WDS) detectors at Heidelberg University with data reported as wt.% oxide and ppmw (parts per million by weight, or μg/g). The operation conditions include an

acceleration voltage of 15 kV, a focused beam with a current of 100 nA, and a working distance of 11 mm. For calibration internal natural and synthetic mineral standards were used and a ZAF correction was applied. Peak counting times for quantitative analyses of the key trace elements (Mg, Ti, V, Cr, Fe and Ga) in corundum of 100 s (Fe), 200 s (Cr) and 300 s (others) and corresponding 50% background integration times translate into limits of detections at a 95% confidence level between 10 ppmw (Mg) and 48 ppmw (Fe). Accuracy was verified by replicate analysis of two multi-doped synthetic corundum crystals (07-0687-08 and 02-1267-21) as well as of natural blue sapphire from Yogo, Montana (Y-1203), and a pure Al_2O_3 blank (16-0524-01) distributed by the Gemological Institute of America (GIA). Relative deviations between EMPA and certified values are +24% for Mg (112 ppmw), +10% for Ti (232 ppmw), −2.9% for V (195 ppmw), +12% for Cr (1892 ppmw), +6.0% for Fe (3357 ppmw), and −4.9% for Ga (130 ppmw) as determined for the reference corundum crystals with the highest abundances (certified values in parentheses).

Phase identification in thin section was aided by Raman microscopy, especially to distinguish between sillimanite and andalusite. A WITec alpha 300R Raman spectrometer equipped with a 532 nm laser was used for thin-section mapping at the Institute of Earth Sciences, Heidelberg University. A Zeiss EC Epiplan 100×/0.9 objective was employed with a laser power of 15 mW. Spectra were recorded with a spectrometer grating of 1200 grooves mm^{-1} for a large area scan with a dwell time of 0.5 s per pixel and the phases

Fig. 3 Selected backscattered electron images of sapphire (Crn = corundum) in lithic ejecta from samples **A** syenite (CSK-04, Emmelberg), **B** hornfels (CSK-06, Hüttenberg Tephra), and **C** mica schist (CSK-12, Rockeskyll). Note melt infiltration in **A**, spinel-free halos surrounding corundum in **B**, and poikilitic corundum overgrowing biotite foliation in **C**. Micro-Raman map (**D**) of sample CSK-05 (Laacher See Tephra) showing intergrowth between sillimanite (Sil) and andalusite (And). Other mineral abbreviations: Bt = biotite, Ilm = ilmenite, Nph = nepheline, Rt = rutile, Sa = sanidine, Spl = spinel
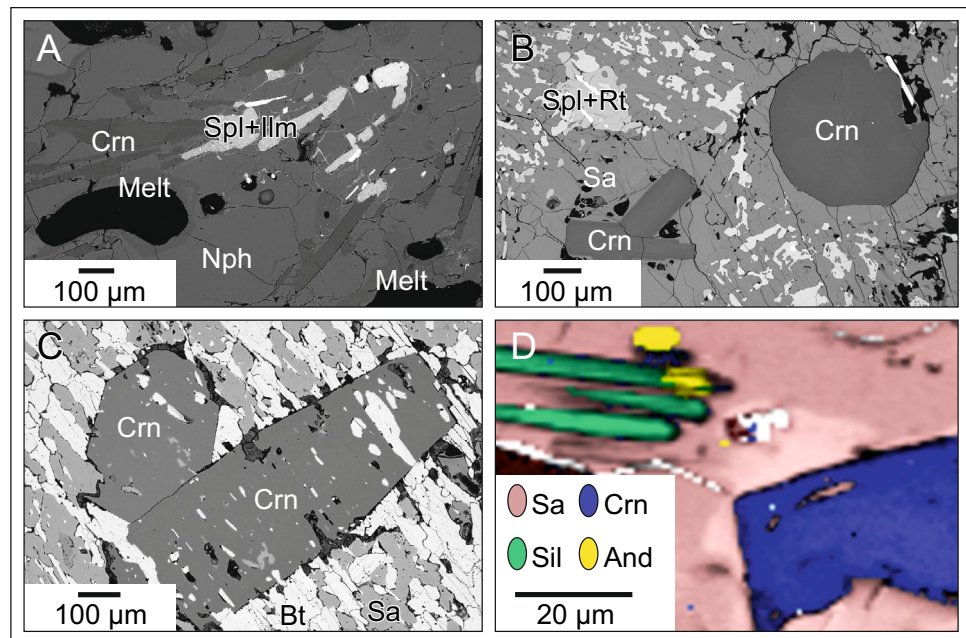
mapped using the WITec True Component Analysis function (Fig. 3D).

Secondary ionization mass spectrometry (Be)

Reconnaissance Be SIMS analyses were performed by using a primary $^{16}O^-$ beam at 23 keV and with ~1 nA intensity focused to a spot size of ~10 μm in diameter. Prior to analysis, the samples were pre-sputtered for 30 s. Intensities of $^9Be^+$ and $^{27}Al^{3+}$ were detected at a mass resolving power (MRP defined at 10% of the peak height) of ~1600 in five cycles totaling 50 and 20 s, respectively, in a single EM by electrostatic peak switching using a deflector located after the magnet (DSP2x). Eifel sapphire was calibrated against a multi-doped synthetic corundum reference material 02-1267-21 (Stone-Sundberg et al. 2017) developed by GIA. GIA specifies the concentration of 02-1267-21 as 2.58 ppmw. Relative standard deviation (RSD) of all 02-1267-21 measurements was 2.6%.

Isotopic analysis

Secondary ionization mass spectrometry (U–Pb)

U–Pb dating of rutile and zircon inclusions in sapphire was performed on a CAMECA IMS 1280-HR ion probe at Heidelberg University by using a primary $^{16}O_2^+$ beam focused to a spot size of 30 μm for rutile (~50 nA) and a primary $^{16}O^-$ beam focused to a size of 20 μm (~5 nA) for zircon. O_2-flooding was applied in both cases to boost Pb yields, and the mass spectrometer was tuned to an MRP of 6000 to resolve interferences on Pb. After a pre-sputtering

time of 20 s, secondary ions were counted with an electron multiplier (EM) over 10 cycles (Schmitt and Zack 2012; Schmitt et al. 2023b). Reference materials R10b (U–Pb age of 1090 ± 5 Ma; Luvizotto et al. 2009) and AS3 (U–Pb age of 1099 ± 1 Ma; Paces and Miller Jr 1993) were used for rutile and zircon, respectively. Model isochrons in a Tera-Wasserburg concordia diagram were calculated for an anthropogenic $^{207}Pb/^{206}Pb$ value of 0.877 (Kern et al. 2021).

Secondary ionization mass spectrometry (O-isotopes)

High spatial resolution oxygen isotope analyses by SIMS were performed on a CAMECA IMS 1280-HR at the Heidelberg Ion Probe (HIP) laboratory by using an ~1–2 nA primary $^{133}Cs^+$ beam focused to ~5 μm with a raster size of 10 μm. Intensities of $^{16}O^-$ and $^{18}O^-$ were detected simultaneously over 15 cycles (4 s each) in two Faraday cups (FC) with 10^{10} and 10^{12} Ω resistors by maintaining a constant magnetic field with nuclear magnetic resonance probes. Samples were pre-sputtered for 30 s after which automatic beam centering (field and contrast apertures) was performed. A normal-incidence electron flood gun was tuned for optimal charge compensation during the analysis. Ten to 15 spot measurements on unknowns were bracketed by replicate analyses of corundum reference HD-LR1 (Vienna Standard Mean Ocean Water VSMOW $\delta^{18}O = 18.40 \pm 0.14$, 95% confidence interval; Schmidt et al. 2024) to monitor instrument drift, geometry-, and topography-effects and to correct for instrumental mass fractionation. Analytical uncertainties were estimated from the standard deviation of bracketing

analyses of HD-LR1 reference material and were on average for each mount between 0.30 and 0.48‰, 2 SD).

Results

Ejecta clast petrology

Examined sapphire-bearing samples from Laacher See (CSK-05) and Hüttenberg Tephra (CSK-06) locations closely match the description of metasedimentary hornfels xenoliths in Wörner et al. (1982) and Grapes (1986). Both share the mineral paragenesis of sanidine + sillimanite + corundum + hercynitic spinel. CSK-06 contains abundant relict biotite, whereas biotite is absent in CSK-05 (Fig. 3B). Sample CSK-05 comprises oligoclase in addition to sanidine. Accessory ilmenite, rutile, and zircon are present, but muscovite and quartz are lacking, and melt is generally absent. Raman mapping of CSK-05 (Fig. 3D) identified partial replacement of sillimanite needles by andalusite requiring pressures <375 MPa (Holdaway and Mukhopadhyay 1993) translating into formation depths <14 km for a crustal rock density (2700 kg/m^3). In CSK-06 (Fig. 3B), large (up to ~500 μm) sapphire crystals are often intergrown with rutile and surrounded by whitish halos of sanidine in a dark matrix consisting of spinel, sanidine, sillimanite, and biotite. The sample from Rockeskyller Kopf (CSK-12) is clearly metasedimentary in origin and it resembles the spotted mica schist described in Wörner et al. (1982). This rock is rich in biotite, displays a strong foliation, and contains pervasive high-Si glass. Two generations of sapphire are present, one pseudomorphic after andalusite (?), and the other porphyroblastic where crystals grew obliquely to the foliation (Fig. 3C) and roughly perpendicular to a mafic vein that crosscuts the metasedimentary clast. The sample from Radersberg (CSK-17) also belongs into this category, although it was too small to prepare a thin section. Although weakly schistose, it is more leucocratic than mica schist, and therefore classified as a metapsammite (Table 1). A third category of sapphire-bearing clasts is rich in sodic alkali feldspar (CSK-04; Emmelberg) or sanidine + oligoclase (CSK-30; Bellerberg). Both contain abundant vesiculated glass, but in contrast to partially molten psammitic rocks found as pyrometamorphic xenoliths (sometimes termed buchites; Wörner et al. 1982), they are quartz-free and therefore named here as syenites (sometimes also termed sanidinites). Embedded in a matrix of nepheline, sapphire in clast CSK-04 (Emmelberg) is lath- to needle-shaped (up to ~0.2 mm × 2.0 mm) and partially replaced by an hercynite-magnetite intergrowth. Ilmenite is present in accessory amounts (Fig. 3C). Sapphire in syenite CSK-30 (Bellerberg) forms millimeter-sized grains that are mantled by hercynitic spinel when in contact to a melt phase; when bordering feldspar, sapphire lacks reaction textures

and subhedral shapes are partly preserved. Besides feldspar, leucite and nepheline are also present in CSK-30 in small amounts. Biotite in CSK-30 is almost completely replaced by fine-grained magnetite-ilmenite intergrowths as ghost phenocrysts. Accessory zircon is present in CSK-04 and -30.

Geochronology of rutile and zircon inclusions in Eifel sapphire

Individual ^{206}Pb/^{238}U ages for inclusions in detrital sapphire grains (rutile $n = 7$, zircon $n = 1$) are imprecise due to low radiogenic Pb contents, but collectively, with one exception, indicate Quaternary ages (Fig. 4; Supplementary Table 1). Within uncertainty, most ages overlap with a 60 ka model isochron. This age corresponds to a prevalent age in Laacher See detrital zircon which dominates the drainages from which the inclusion-bearing sapphire grains were recovered (Schmitt et al. 2023b). Only one rutile inclusion in a pink colored host from Nitzbach appears to be older, and plots on a 25 Ma model isochron consistent with formation in the wake of the Neogene Hocheifel volcanism (Fig. 4). This is consistent with the comparatively large fraction of detrital zircon in the Nitzbach drainage that is derived from evolved Hocheifel volcanic rocks (Schmitt et al. 2023b).

Eifel sapphire trace elements

Quantitative trace element measurements of Mg, Ti, V, Cr, Fe, and Ga (Figs. 5, 6, 7; Supplementary Table 2) reveal that
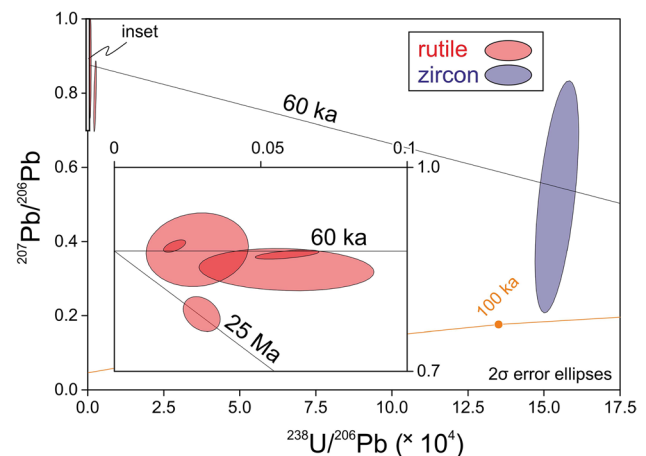

Fig. 4 ^{207}Pb/^{206}Pb vs. ^{238}U/^{206}Pb diagram showing data for rutile and zircon inclusions in Eifel detrital sapphire. Rutile inclusion bearing grains were recovered from Brohlbach ($n = 4$), Nette ($n = 1$) and Nitzbach ($n = 2$); one zircon inclusion was from Nette. Data are plotted uncorrected for common Pb; they therefore represent mixtures between radiogenic and common Pb components. Model isochrons of 60 ka (corresponding to the onset of zircon crystallization in the Laacher See) and 25 Ma through an anthropogenic common Pb composition of 0.877 are plotted for comparison
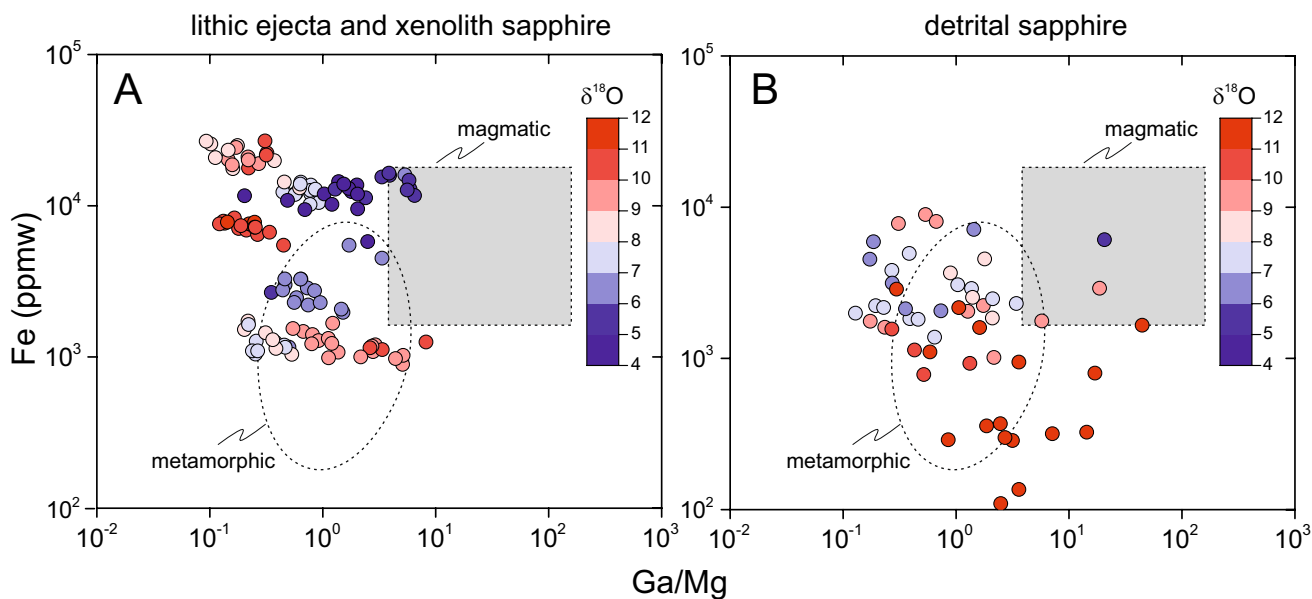
Fig. 5 Fe vs. Ga/Mg trace element classification diagrams for sapphire from lithic ejecta and xenoliths (**A**) and detrital (**B**) samples with fields for magmatic and metamorphic sapphire after Peucat et al. (2007). Color map uses δ^{18}O average values for the same grains and grain domains

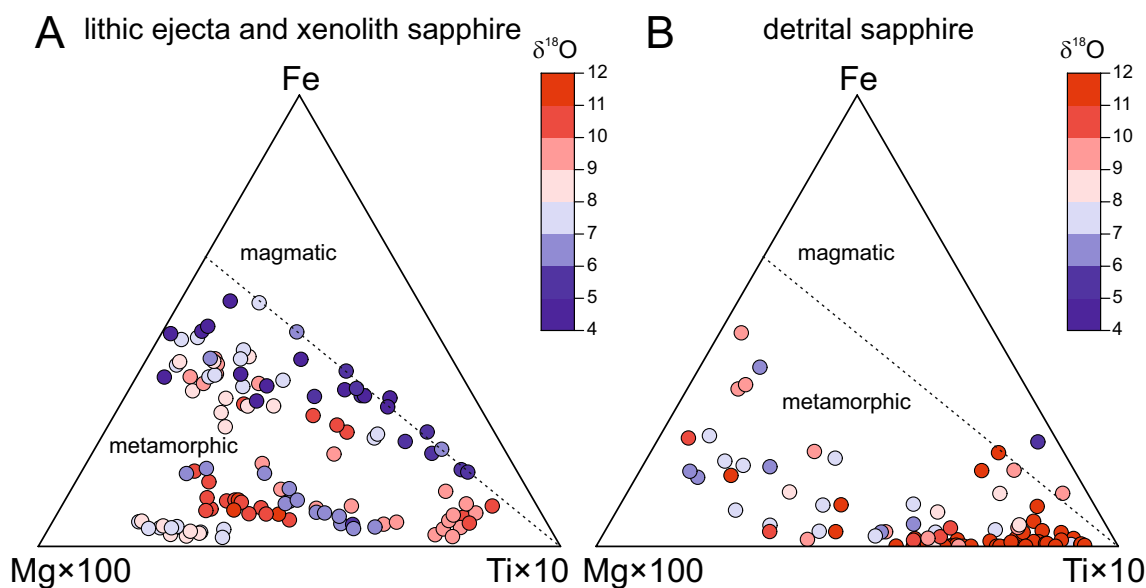**Fig. 6** Fe–Mg × 100–Ti × 10 ternary classification diagrams for sapphire from lithic ejecta and xenoliths (**A**) and detrital (**B**) samples. Subdivision between magmatic and metamorphic sapphire after Peu- cat et al. (2007). Color map uses δ^{18}O average values for the same grains and grain domains

Fe (893–26,800 ppmw) is typically the most abundant non-stochiometric component in primary WEVF and EEVF sapphire. Sapphire from mica schist displays the lowest abundances (893–1670 ppmw), whereas sapphire from hornfels (Hüttenberg Tephra) shows comparatively high levels of Fe (17,600–26,800 ppmw). Titanium (<22–5890 ppmw) and Mg abundances (<12–643 ppmw) vary unsystematically across all petrologic types. In terms of V concentrations,

sapphire from syenite (Bellerberg) along with the sapphire from hornfels in a tephrite lava (Mendig) have comparatively high abundances (86–816 ppmw) relative to the other types (<16–505 ppmw). Sapphire from syenite (Emmelberg) and hornfels (Laacher See) stand out by low Cr concentrations below the detection limit, whereas Cr is detectable at higher levels up to 826 ppmw in the other samples. Gallium abundances of all samples are similar and range from values
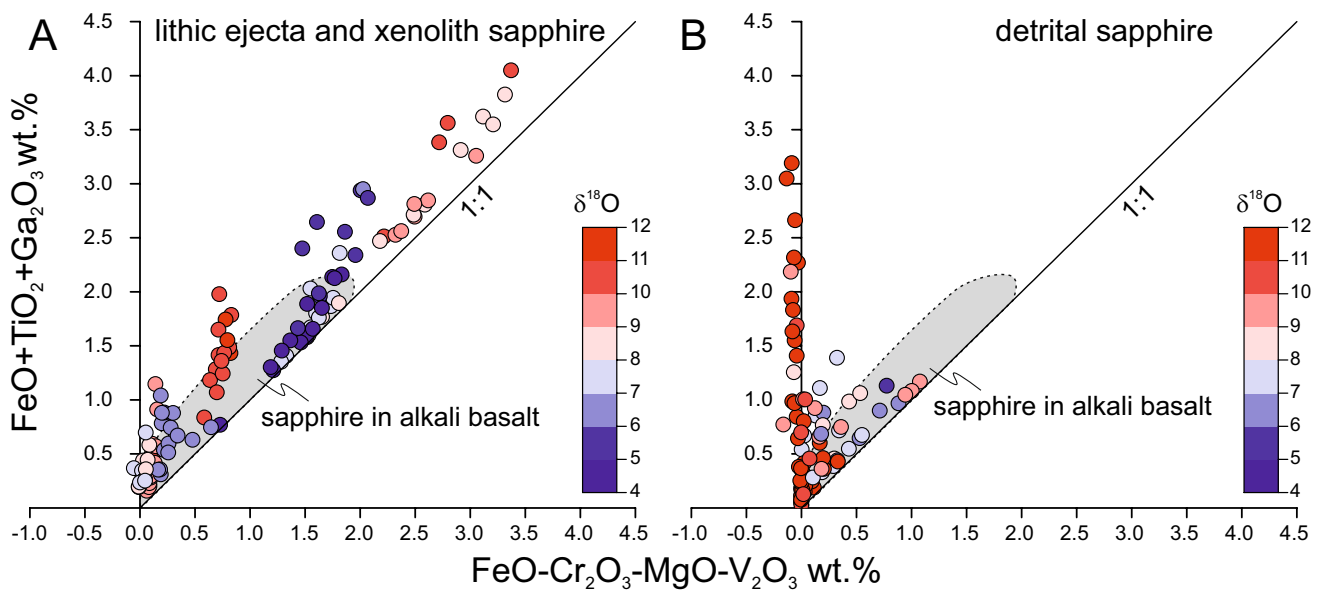
Fig. 7 $FeO–Cr_2O_3–MgO–V_2O_3$ vs. $FeO+TiO_2+Ga_2O_3$ diagram (in wt.%) for classifying corundum deposits with field for sapphire xenocrysts in alkali basalt and lamprophyre (Giuliani et al. 2014). Lithic ejecta and xenolith (**A**) and detrital (**B**) sapphire compositions are plotted for comparison; color map uses $\delta^{18}O$ average values for the same grains and grain domains

below the detection limit to 492 ppmw. Trace element compositions of secondary sapphire from river sediments largely overlap with those from ejecta clasts, and they lack clear systematic differences between sites in the WEVF and EEVF. The exception is detrital sapphire from Brohlbach where many grains are comparatively low in Fe, V, and Cr, whereas particularly dark blue sapphire grains have among the highest Ti and moderately elevated Mg abundances of the entire population. Most examined sapphire crystals lack detectable chemical zoning. Some sapphire crystals from hornfels, however, are chemically zoned as indicated by BSE contrasts between core and rim domains which correlate with high Fe and Ti abundances in the core (Fig. 8). Magnesium, V, and Cr, by contrast, are homogeneously distributed across the boundary between the grains' core and rim.

Trace element ratios, either in bivariate or ternary diagrams (Figs. 5, 6, 7), are used for discrimination of sapphire origins, with magmatic sapphire having higher Fe (up to ~10,000 ppmw for sapphire from syenitic rocks) and higher Ga/Mg (>10) compared to metamorphic sapphire (Peucat et al. 2007). These authors attributed depletion of Ga in regional metamorphic rocks to extraction of Ga via F-rich melts in granulitic restites, whereas Ga is expected to become enriched upon differentiation of alkaline magmas based on the negative correlation between Ga and MgO in igneous rocks (Kato et al. 2017). Magmatic sapphire is also characterized by high Fe/Mg (>100) compared to metamorphic sapphire (Giuliani et al. 2014). Discrimination diagrams (e.g., Groat et al. 2019; Peucat

et al. 2007) on one hand indicate mostly metamorphic origins for the Eifel sapphires (e.g., with Ga/Mg < 10 except for syenitic clasts from Emmelberg), whereas on the other hand Fe abundances are elevated relative to the metamorphic fields at least for many of the ejecta- or lava-hosted sapphire crystals (Fig. 5). This also holds for the Fe–Mg×100–Ti×10 ternary diagram (Peucat et al. 2007), where most data fall into the metamorphic field (Fig. 6). Nonetheless, data with low $\delta^{18}O$ (4–6‰) generally overlap with the "sapphire in alkali basalt" field of Giuliani et al. (2014), although they display more variability than delineated by this field (Fig. 7). In this, the Eifel sapphires share the same ambiguities regarding their classification as other occurrences in the Paleogene Central European Volcanic Province including locations in the Siebengebirge, the Ohře Graben, and the Western Carpathians, which also fall outside many of the existing trace element classification fields (Baldwin et al. 2017; Seifert et al. 2014; Uher et al. 2012).

Lastly, we explored Be abundances in clast-hosted or xenocrystic sapphire, which are <19.7 ppmw, and with the on average most elevated values found in syenite-hosted sapphire (Emmelberg) which also displays the lowest Cr/Ga. The bulk of the analyses, however, is between ~1 and 0.01 ppmw, consistent with expected low abundances of untreated natural corundum (Emmett et al. 2003). As none of the sampled crystals was treated for color enhancement, the value of 19.7 ppmw Be is tentatively marked as an upper limit for natural corundum.
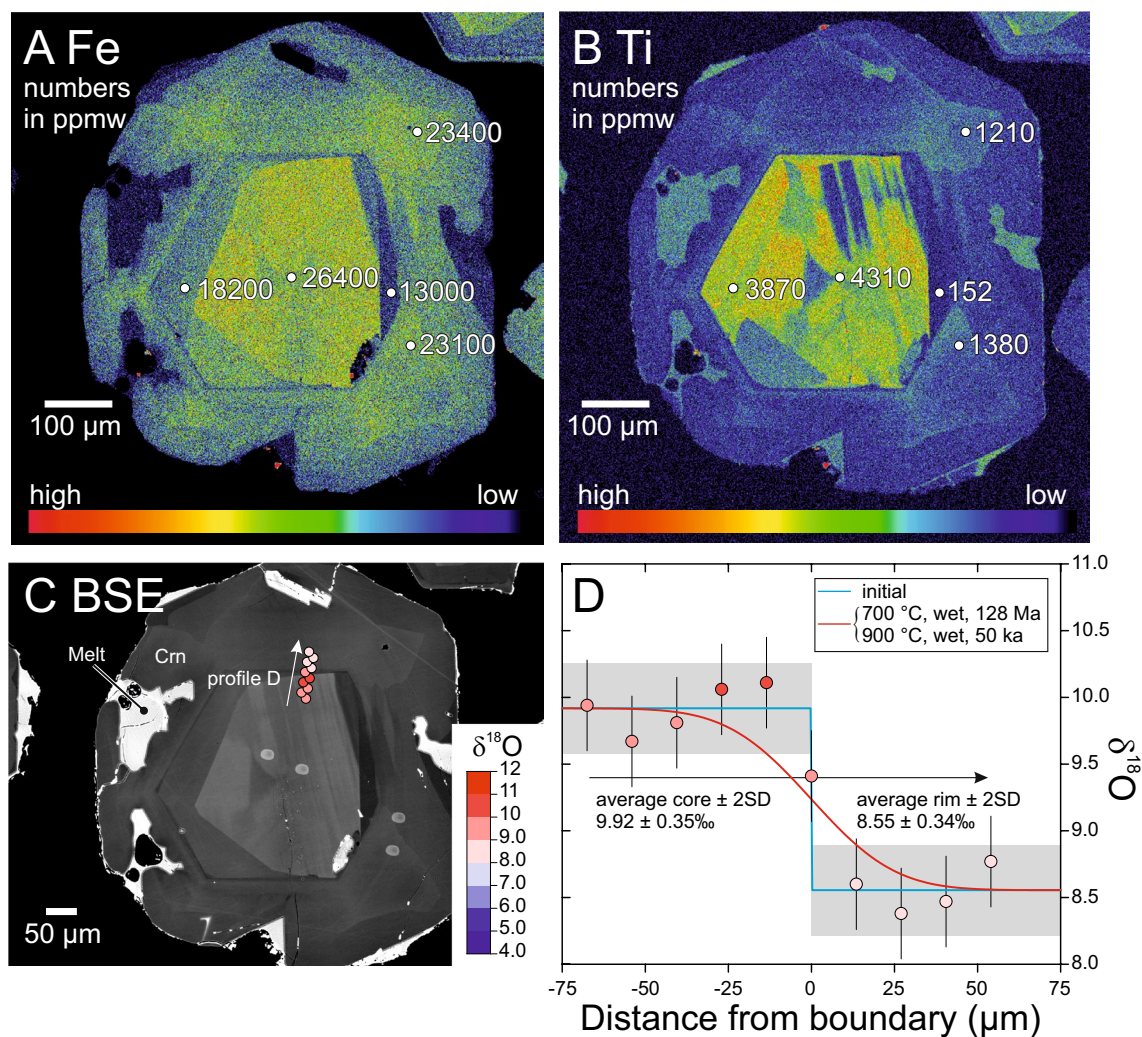
Fig. 8 EMPA raw intensity maps for Fe (**A**), Ti (**B**) and backscattered electrons (BSE; **C**) for sapphire grain 6 extracted from hornfels (CSK-06, Hüttenberg Tephra). Location of quantified EMPA spots (values in ppmw) and O-isotope profiles are shown in **A**+**B** and **C**, respectively, with data and diffusion model plotted in **D** (colors as in Figs. 4, 5, 6, 7). EMPA map was acquired under the following conditions: 15 kV, 50 nA, focused beam, dwell time 20 ms, and 800×800 points/pixel

Eifel sapphire oxygen isotopes

As with trace elements, O-isotopic data of WEVF and EEVF samples form a continuum, even though individual samples generally display a limited range (Fig. 9; Supplementary Tables 2 and 3). The lowest and highest $\delta^{18}O$ values for ejecta clast- and lava-hosted sapphire were detected in the WEVF. Sapphire in syenite ejecta clasts (Emmelberg) shows the lowest values which average $4.84 \pm 0.40‰$ (2SD, $n=20$) and $5.77 \pm 0.40‰$ (2SD, $n=9$) in two separate clasts. The highest average values for sapphire were determined at $9.64 \pm 0.57‰$ (2SD, $n=20$) and $10.80 \pm 0.54‰$ (2SD, $n=15$) in mica schist (Rockeskyll) and metapsammite (Radersberg), respectively (Fig. 9A).

The $\delta^{18}O$ values of EEVF sapphire (Fig. 9B) show a narrower spread of <3‰, with samples from syenite (Bellerberg) displaying the lowest values (average = $6.45 \pm 0.55‰$; 2SD, $n=17$), consistent with the WEVF syenites. The O-isotopic signatures of hornfels (Mendig, Laacher See) are identical with average values of $7.89 \pm 0.43‰$ (2SD, $n=14$) and $7.89 \pm 0.48‰$ (2SD, $n=14$), respectively (Fig. 9B). Some sapphire analyses from hornfels (Hüttenberg) overlap with those from Laacher See and Mendig in $\delta^{18}O$ (Fig. 9B), but most sapphire is isotopically heavier with an average isotopic composition of $9.21 \pm 1.22‰$ (2SD, $n=14$). This sample also displays a significantly larger internal spread compared to other clasts (Figs. 8, 9B).

Modern river sediments in the EEVF contain significantly more sapphire than sediments in the WEVF as reflected by the different totals of examined grains (WEVF: 20, EEVF: 80; Table 1). Detrital sapphire from

Fig. 9 SIMS O-isotopes summary for lithic ejecta and xenoliths (**A**) and detrital (**B**) samples from WEVF and EEVF. Individual analyses are shown as vertical dashes, probability density functions for each sample as half-violin plots

Discussion

Hypotheses on corundum formation in alkali basaltic associations
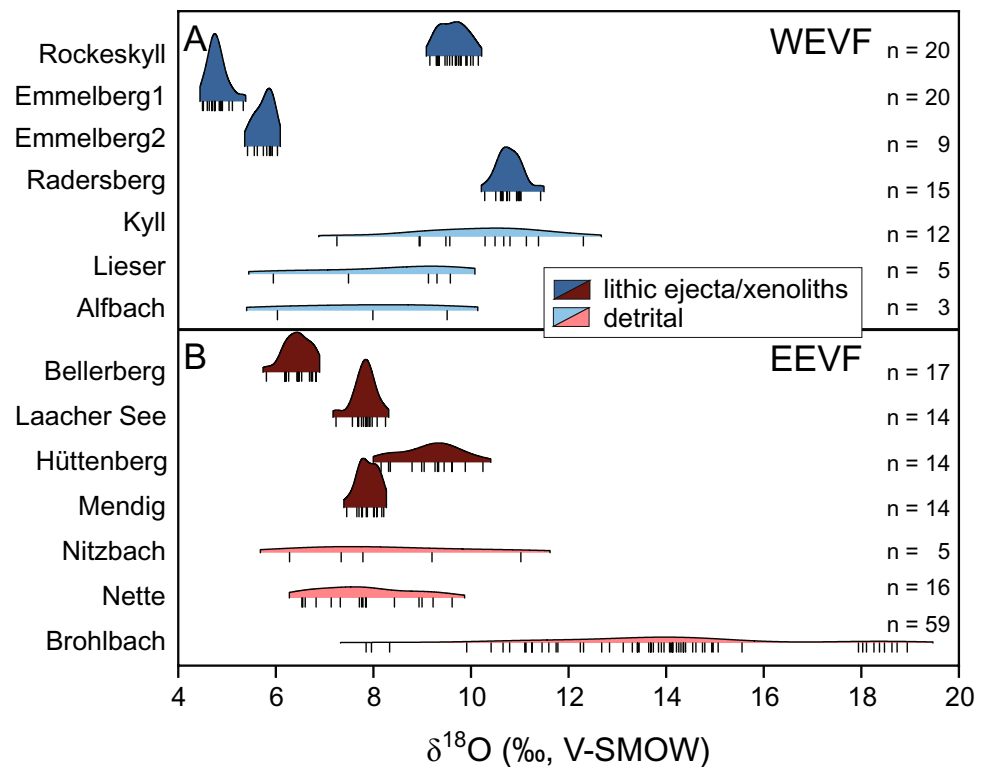
the WEVF (Fig. 9A) shows a $\delta^{18}O$ range from 5.96‰ (Lieser) to 12.31‰ (Kyll). The $\delta^{18}O$ data of detrital grains from EEVF (Fig. 9B) display three peaks at approximately 7.5, 14.5, and 18.5‰, with a maximum value of 18.94‰, respectively (Table 1). The peak at 7.5‰ overlaps with sapphire compositions from Laacher See hornfels, whereas the highest isotopic values that are prevalent in Brohlbach sediments have no equivalent in any of the other Eifel samples. The overall range of $\delta^{18}O$ of Eifel sapphire overlaps closely with data for the Massif Central (4.4–13.9‰; Giuliani et al. 2009) with only the higher values from Brohlbach being distinct. In fact, the overall range of $\delta^{18}O$ in Eifel sapphire is only marginally smaller than that of a global compilation for sapphire ranging from −0.3 to 19.9‰ (Wong and Verdel 2018), where only a small fraction of low-$\delta^{18}O$ (<<5.5‰) sapphire crystals in the global data set is not represented in the Eifel data. Indexing $\delta^{18}O$ in these commonly applied sapphire trace element discrimination diagrams (Figs. 5, 6, 7) reveals that the extremes in the overall $\delta^{18}O$ range of 4–6‰ and 10–19‰ are also most clear-cut in their respective magmatic and metamorphic assignments. Intermediate $\delta^{18}O$ values between 6 and 10‰, however, are generally distributed over the magmatic vs. metamorphic fields in trace element classification diagrams.

The frequent association of alkali basaltic volcanic fields and corundum has long been enigmatic. Although these deposits are classified as magmatic (Giuliani et al. 2014), corundum found in alkaline basaltic fields sensu lato can be genetically attributed to magmatic, e.g., when derived from syenitic xenoliths, or metamorphic sources, where the source are pre-existing crustal rock (e.g., gneiss, skarn, marble, or pegmatitic intrusives; Giuliani et al. 2014). To complicate classification, corundum is often only recovered as xenocrysts in mafic volcanic host rocks, although there is general agreement that these volcanic hosts are merely the agent through which corundum was transported from its source to the surface (e.g., Baldwin and Ballhaus 2018). To resolve the formation processes of corundum in alkaline basaltic fields, different methods have been applied in the literature: if found in the context of the source rock, petrography and mineral parageneses have provided key insights along with the study of fluid and mineral inclusions, including dating of enclosed zircon

and rutile, (e.g., Baldwin et al. 2017; Coenraads et al. 1990; Palke et al. 2017; Sorokina et al. 2017; Xu et al. 2021), but also trace elements (e.g., Sutherland et al. 1998; Peucat et al. 2007; Wong et al. 2017), O-isotopes (e.g., Giuliani et al. 2009; Wong and Verdel 2018), and noble gasses (e.g., Guo et al. 2022) have yielded important clues. Collectively, these studies adhered to two main hypotheses: (1) corundum precipitated from highly fractionated silicate-carbonatitic melts that were derived from the mantle and differentiated in the upper mantle or lower crust (e.g., Sutherland et al. 1998; Uher et al. 2012), potentially reaching exsolution of a CO_2-rich melt (Baldwin et al. 2017), or (2) corundum is an accidental component in mafic alkali melts that was scavenged from Al-rich crustal rocks such as metasediments (Levinson and Cook 1994), anorthosites (Palke et al. 2017), or hybridized granitic-carbonatitic rocks (Guo et al. 1996). Inclusion ages overlapping those of the volcanic hosts (e.g., Coenraads et al. 1990) indicate that crustal heating and metasomatism in the metamorphic scenario is often directly related to the same magmatic pulse that also triggered alkaline basaltic volcanism.

Hypotheses for corundum formation in other fields within Central European Volcanic Province that are the geographically and geologically closest analogs for the Eifel also fall into these categories. The Siebengebirge is located only ~35 km NW of the center of the Eifel, but in contrast to the Eifel, volcanism is restricted to the Paleogene (e.g., Lippolt 1983). Zircon inclusions in sapphire from the Siebengebirge dating to c. 25 Ma clearly indicate formation contemporaneous with local volcanism, and CO_2-rich fluid inclusions indicate entrapment at >12 km depth (Baldwin et al. 2017). The coexistence of two types of melts in individual inclusions, one identified as a carbonated silicate melt, and the other as aluminous phonolite, suggests sapphire formation from a highly evolved immiscible carbonatitic melt (Baldwin et al. 2017). Sapphire was then enclosed as a xenocryst in an alkaline basaltic melt where it reacted to form spinel coronas (Baldwin et al. 2017). For the Ohře Graben, placer sapphire was classified based on the inclusion paragenesis and trace elements into magmatic and metamorphic types (Seifert et al. 2014). Magmatic inclusions include spinel, ilmenite, magnetite, rutile, and zircon, whereas metamorphic inclusions comprise graphite and chlorite; as a magmatic source, highly evolved alkaline silicate melts were proposed (Seifert et al. 2014). The only detailed O-isotopic study for the Central European Volcanic Province so far was for sapphire from Massif Central which revealed a population with low $\delta^{18}O$ (4.4–6.8‰) that was presumably derived from felsic melts crystallizing in the upper mantle, whereas a second population inherited its elevated $\delta^{18}O$ values (7.6–13.9‰) from metamorphic crustal source rocks including schists, gneisses, and skarns (Giuliani et al. 2009). A small number

of sapphire crystals ($n = 5$) was also analyzed for $\delta^{18}O$ from occurrences in the Western Carpathians (Slovakia). These crystals occur mainly in placers, but sapphire is also rarely preserved in xenoliths of syenitic-anorthoclasic composition in regional Pleistocene alkali basalts (Uher et al. 2012). Mantle-like $\delta^{18}O$ signatures (3.80–5.85‰) were attributed to crystallization in fractionated melts at upper mantle or lower crust depths (Uher et al. 2012). Based on elevated Cr and Mg abundances, a second population was interpreted to be of xenocrystic origin derived from metamorphic or metasomatic crustal source rocks (Uher et al. 2012).

As a previously unstudied location in the Central European Volcanic Province, the Eifel shares many similarities with these other location regarding its sapphire population: sapphire occurs in syenitic (sanidine ± oligoclase ± leucite ± nepheline ± biotite ± magnetite) and metasedimentary (sanidine + sillimanite + spinel ± oligoclase ± biotite) host rocks (Figs. 2, 3), which are typically described as magmatic and metamorphic endmembers for corundum-bearing host rocks in other fields, respectively. Ages for zircon and rutile inclusions in the subset of dated sapphire crystals (Fig. 4) are also coeval with alkaline mafic volcanism, which is Quaternary in the WEVF and EEVF, with one potential exception suggesting a Paleogene age associated with Hocheifel volcanism. Lastly, trace element and O-isotopic compositions in corundum, where available from other locations in the Central European Volcanic Province, are also like those from the Eifel, especially regarding the wide range of elemental and isotopic compositions that indicate multiple formation pathways. These similarities identify the Eifel as a representative location for sapphire genesis in intracontinental magmatic settings, although gem-quality sapphire megacrysts have not been described for the Eifel (cf. Massif Central).

Detrital and volcanic-hosted sapphire sources in the Eifel

In comparison to other locations in Central Europe or worldwide where sapphire is found within alkaline basaltic fields (see reviews in Giuliani and Groat 2019; Groat et al. 2019), the Eifel as a comparatively young and active system has the advantage that besides the detrital and xenocrystic populations, volcanic ejecta with sapphire-bearing host rocks are accessible, and thus a petrographic context is preserved. The sampling of these ejecta is necessarily punctuated due to them being scarce. Moreover, they are often pyrometamorphically overprinted due to their entrainment in hot mafic magma prior to eruption. By contrast, detrital sapphire from the Eifel lacks this petrographic context, but we include detrital sapphire because sampling is more representative on a regional scale.

Comparison between volcanic-hosted and detrital population reveals close similarities in color, morphology, trace

element inventory, and O-isotopic composition. Using $\delta^{18}O$ as a fingerprint (Fig. 9), the isotopic ranges for the WEVF are very similar for detrital (5.96–12.31‰) and volcanic-hosted sapphire (4.52–11.44‰). The same holds for EEVF Nette and Nitzbach drainages (6.29–11.03‰) which overlap with hornfelsic sapphire from Laacher See Tephra (7.30–8.32‰). The exception is high $\delta^{18}O$ detrital sapphire with values up to 18.94‰ in the Brohlbach sediment that exceed those for the potential source of Hüttenberg Tephra with a maximum value 10.29‰ (Fig. 9). While this could reflect sampling bias with only a single clast investigated from Hüttenberg Tephra, it is also possible that detrital sapphire was derived from volcanic rocks or ejecta in deposits of the Rieden complex or from the Glees and Dümpelmaar tephras, which represent younger eruptions from the vents within or adjacent to the Wehr complex (Schmitt et al. 2023b) that were not sampled here. With this caveat, we can combine the information from both sapphire populations to evaluate potential formation mechanisms.

Oxygen-isotopic typology of sapphire in alkali basaltic volcanic fields

Oxygen with ~50 wt.% in most rocks and minerals is the most abundant element in the silicate Earth, and therefore significant mass transfer is required to shift their O-isotopic compositions. Based on existing calibrations for temperature-dependent equilibrium isotopic fractionation between corundum and silicates, corundum at 700 °C is depleted in ^{18}O by ~1.9‰ relative to albite (Krylov and Evarestov 2018; Qin et al. 2016) and by ~2.2‰ relative to a phonolitic melt (nepheline syenite in Table 6 of Zhao and Zheng 2003). The upper limit for the magmatic endmember $\delta^{18}O$ compositions is derived from values for Quaternary Eifel volcanic rocks, where sanidine in evolved Laacher See pumice ranges between 6.6 and 8.0‰ (Wörner et al. 1987). The lower limit for the crustal endmember is from bulk values for slate and mica schist of 11.7 and 14.0‰, which are also the likely crustal contaminants that have caused a shift in the parental Laacher See magma from initially 5.5‰ to higher values in more evolved magmas (Wörner et al. 1987). By contrast, a granulite xenolith value of 7.2‰ (Wörner et al. 1987) implies that lower crustal $\delta^{18}O$ is too low to be a viable contaminant. Accounting for isotopic fractionation at 700 °C, sapphire with values <6‰ is therefore consistent with crystallization from differentiated magmas whereas those with values >10‰ likely formed within pure crustal rocks.

Magmatic crystallization is the most likely scenario for sapphire from syenite, which are best represented by Emmelberg samples (CSK-04 and -16, $\delta^{18}O = 4.52$–6.03; Table 1; Fig. 9). Based on their O-isotopic compositions, these are assigned to the magmatic sapphire endmember (Type 1). Type 1 also displays the lowest Cr/Ga and

highest Fe/Mg values, along with the highest Be abundances. It remains unclear, however, if uncontaminated mantle-derived phonolite will become saturated in sapphire in its magmatic evolution, although previous studies advocated this based on MELTS equilibrium crystallization simulations (Sutherland et al. 1998). The newer rhyolite-MELTS model (Gualda et al. 2012), however, failed to reproduce these results, but we also caution that the MELTS simulation software is not calibrated for highly differentiated SiO_2-undersaturated, H_2O, CO_2, and SO_2-rich melts such as those of Laacher See (e.g., Harms and Schmincke 2000). Instead, it appears more likely that addition of peraluminous partial melts derived from a pelitic protolith (Grapes 1986), or alkali loss due to exsolution of a carbonatitic melt would shift a residual phonolitic melt into the corundum stability field (e.g., Upton et al. 1999). This likely restricts sapphire crystallization to the largely solidified margins of a magma reservoir in contact with Al-rich metasedimentary wall rocks. Such a scenario is also consistent with the absence of corundum in even the most evolved trachyte or phonolite pumice from the Eifel (e.g., Wörner and Schmincke 1984).

Sapphire from mica schist, metapsammite, and hornfels (Rockeskyll, Radersberg, and Hüttenberg) are attributed to contact metamorphic reactions in metasedimentary wall rocks that involved breakdown of muscovite and biotite producing corundum and melt (Grapes 1986). This second O-isotopic endmember (Type 2) is defined by average O-isotopic compositions of $\geq 10‰$. Type 2 sapphire is also characterized by elevated Cr/Ga and low Fe/Mg. When the SiO_2-rich partial melts are extracted from the metasedimentary source rock, corundum can form in the Al_2O_3-enriched restitic component in a 'degranitization' scenario as described by Wörner et al. (1982). Depending on these processes, O-isotopic compositions may deviate slightly from the bulk because of minor isotopic differences in the constituting minerals of regional metamorphic source rock such as mica schist or gneiss (Garlick and Epstein 1967).

Based on intermediate $\delta^{18}O$ values between ~6 and 10‰, the remaining sapphire-bearing rocks including some syenites and hornfels (Bellerberg, Laacher See, Mendig) are grouped into Type 3. Generally, Type 3 sapphire is also intermediate in trace element abundances compared to the other types. Type 3 was only found in the EEVF and it requires a hybrid origin involving mixing between mantle-derived melts and crustal rocks. Lithological type and trace element classifications are broadly consistent for the $\delta^{18}O$ endmembers Type 1 (mostly syenite) and 2 (mostly mica schist), but Type 3 is more ambiguous. This hints at processes operating in late-stage magmatic and contact metamorphic environments that defy a clear-cut separation into magmatic or metamorphic origins.

Sapphire intra-grain zonation

The preservation of O-isotopic zonation in hornfelsic sapphire from the Hüttenberg Tephra (Fig. 8) provides additional insights into the processes leading to corundum formation with hybrid compositions: early formed sapphire has elevated $\delta^{18}O$ of $9.92 \pm 0.35\permil$ (2SD, $n = 5$, average for the interior part of the analyzed profile), close to the value expected for metamorphic corundum. This agrees with typically higher Fe and Ti abundances in sapphire cores relative to rims (Fig. 8), consistent with breakdown of muscovite and biotite in a metasedimentary protolith due to heating in a contact metamorphic aureole (Grapes 1986). At a later stage, the core became rimmed by sapphire with $8.55 \pm 0.34\permil$ (2SD, $n = 4$, average for the outer part) which is comparatively low in Fe and Ti (Fig. 8). In-situ melting of the protolith is insufficient to lower $\delta^{18}O$, because O-isotopic fractionation is small at magmatic temperatures, and anatectic melts largely inherit the isotopic composition of their protolith (e.g., Jung et al. 1998). The approximately $-1.5\permil$ shift from core to rim therefore requires addition of a low $\delta^{18}O$ component, for which the Hüttenberg trachyte magma is the most likely candidate. Hybridization between trachytic and in-situ produced rhyolitic melts would result in precipitation of a sapphire rim with intermediate $\delta^{18}O$ compositions. The presence of partial melt pockets in the hornfels and interfingering between melt and sapphire in its outer domains supports penetration by such a hybrid melt from which a second generation of sapphire crystallized.

The conditions of this hybridization can be further constrained by considering the duration of sapphire crystal residence as inferred from O-isotope diffusion modeling. The diffusivity of O-isotopes in corundum is sluggish, especially at low temperature (Zheng and Fu 1998): diffusion coefficients D at 700 °C (the maximum temperature assumed for sapphire in Hüttenberg Tephra ejecta; Wörner and Fricke 1984) are $\log D = -21.3$ cm^2/s (wet) and $\log D = -28.9$ cm^2/s (dry). In the following, wet diffusion is assumed because phonolite melts such as Laacher See are hydrous (~6 wt.%; Berndt et al. 2001; Harms and Schmincke 2000), and crustal wall rocks contain OH-bearing minerals that break down to produce hydrous peraluminous melts (Grapes 1986). Only entrainment in hot, primitive mafic melt shortly prior to or during eruption could promote dry diffusion, but magma ascent timescales are typically too short (hours–days; Denis et al. 2013) to cause significant diffusion. Under wet conditions at 700 °C, isothermally re-equilibrating the interior of a 500 μm diameter sapphire crystal with an outside reservoir would require an unrealistic protracted duration of c. 1 Ga. Even the sharp isotopic contrast over ± 10 μm across the boundary between core and mantle domains can be preserved at 700 °C over c. 128 Ma, much longer than the duration of Cenozoic volcanism in

the Eifel (Fig. 8). By contrast, this duration reduces to only c. 50 ka at 900 °C of isothermal crystal residence (all for wet diffusion; Fig. 8). The ideal thermal conditions for preservation of step-shaped isotopic contrasts are therefore in low-moderate temperature metamorphic environments, such as at the margin of a mid-upper crustal magma reservoir, where temperatures <700 °C prevail. By contrast, residence at lower crustal to upper mantle depths where ambient temperatures of ~900 °C are reached at 30–40 km in the Eifel (Garcia-Castellanos et al. 2000) would rapidly level any intra-grain O-isotopic differences. Over the known durations of magma presence in the Laacher See system as constrained by the onset of zircon crystallization at c. 63 ka and the eruption at 13 ka (Schmitt et al. 2023b), sapphire residence at 900 °C can therefore be dismissed (Fig. 8). Furthermore, sapphire formation at mantle or lower crustal depths (cf. Sutherland et al. 1998; Uher et al. 2012; Upton et al. 2009, 1999) violates constraints from fluid inclusion barometry (Wörner and Fricke 1984), the presence of andalusite (either as pseudomorphs or a relict grains), and the presence of sapphire-bearing mid- to upper crustal metasedimentary wall rocks in the lithic ejecta clast populations (Schmitt et al. 2017; Wörner et al. 1988; Fig. 10).

Conclusions

Sapphire from the Quaternary Eifel intracontinental volcanic field occurs in xenoliths present in pyroclastic deposits and lava, and in detrital grains in modern river sediment. Rutile and zircon inclusion ages indicate sapphire formation coeval with Quaternary volcanic activity in the WEVF and EEVF, with one detrital sapphire possibly formed in association with Paleogene Hocheifel volcanism. Three sapphire subtypes are classified based on $\delta^{18}O$ compositions as (1) magmatic with $\delta^{18}O$ between ~4 and 6‰ that match bulk phonolite compositions from ~6 to 8‰. This type also displays low Cr/Ga and high Fe/Mg, and they are best represented by sapphire in syenites with the paragenesis sanidine + hercynite ± nepheline; (2) metamorphic with $\delta^{18}O > 10\permil$ and high Cr/Ga and low Fe/Mg. This type includes mica schist and metapsammite hosts with the paragenesis sanidine + oligoclase + sillimanite + corundum + spinel + biotite; high $\delta^{18}O$ detrital sapphire from the Brohlbach river also belong to this group although their origin is uncertain; and (3) intermediate with $\delta^{18}O$ (6–10‰) values and trace element abundances which indicate hybrid origins in metasomatized wall rock surrounding the contact aureole of low-level crustal (5–7 km) magma reservoirs (i.e. hornfels comprising sanidine + sillimanite + corundum + hercynitic spinel ± biotite ± andalusite).

The coexistence of magmatic, metamorphic, and hybrid sapphire suggests a continuum of processes where evolved

Fig. 10 Schematic summary of sapphire formation in mid-upper crustal magma reservoirs of differentiated (tephrite, trachyte, phonolite, and carbonatite) magmas. These magmas are prevalent in the WEVF, but they are also present in small volumes in the EEVF. Primitive mafic melts (foidite and basanite) originated in the mantle with its mineralogy inferred from xenoliths and geochemistry (modified after Schmincke 2007). Major O-isotopic reservoirs (mantle, lower crust LC, middle crust MC, and upper crust UC) and magma compositions are indicated (Kempton et al. 1988; Wörner et al. 1982) with range of sapphire O-isotopes for comparison (this study). Note that mid-upper crustal rocks are viable magma contaminants, whereas lower crustal granulite can be ruled out as the source for high-$\delta^{18}O$ sapphire. Depth scale is variable, and volcano size is unscaled
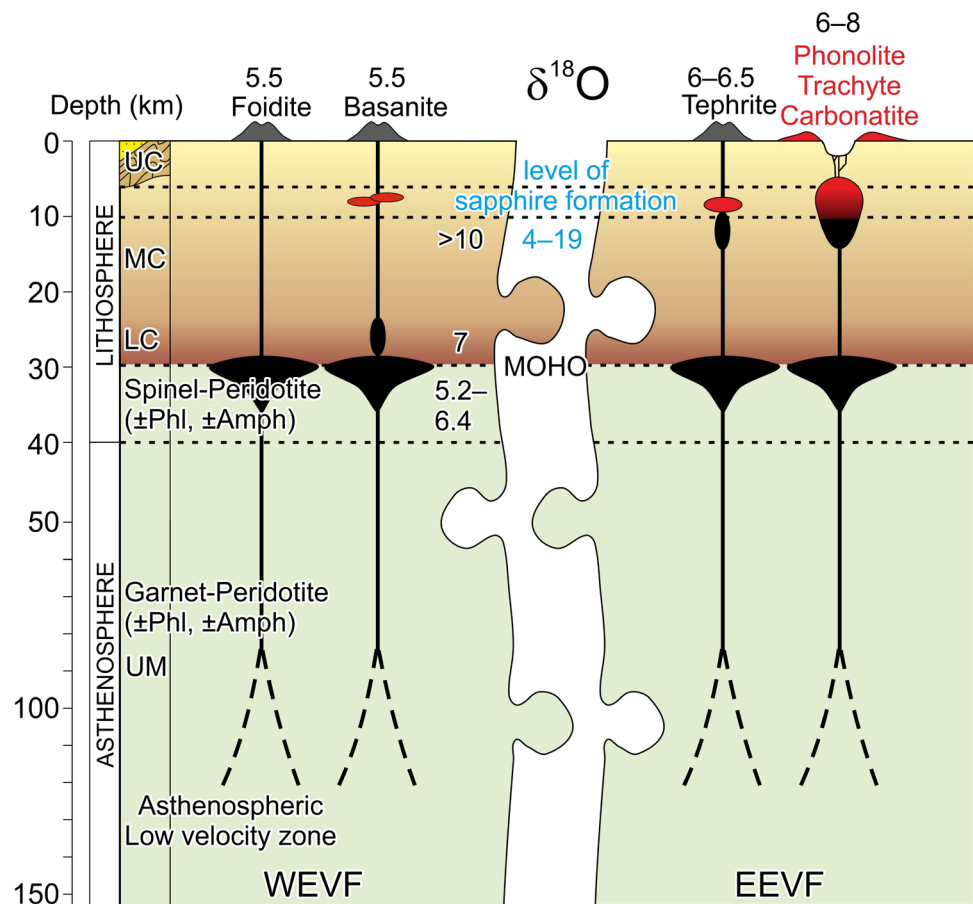
phonolite assimilated metasedimentary wall rocks which conversely became metasomatized and/or heated in a contact metamorphic aureole. Exsolution of a CO_2-and alkali-rich immiscible melt or mixing with peraluminous partial melts aided in shifting contaminated evolved phonolite melt into the corundum stability field. In contrast to previous studies that advocated corundum formation in the upper mantle or lower crust, the available barometric constraints for the Eifel including fluid inclusions, the presence of andalusite, isotopic trends that are consistent with mid-upper crustal metasedimentary contaminants, and the preservation of sharp intra-grain O-isotopic zonation all favor sapphire formation and residence in low-level crustal intrusions where mantle-derived magmas differentiated to volatile-rich alkaline compositions (Fig. 10). Although the wide range of O-isotopic compositions even within a single volcanic field limits the power of $\delta^{18}O$ as a geographical provenance indicator, this study showcases the valuable genetic information that can be extracted from $\delta^{18}O$ analysis of corundum.

Supplementary Information The online version contains supplementary material available at https://doi.org/10.1007/s00410-024-02136-x.

data availability The authors declare that the data supporting the findings of this study are available within the paper and its supplementary information files.

References

Baldwin LC, Ballhaus C (2018) Experimental investigation of the reaction between corundum xenocrysts and alkaline basaltic host magma: constraints on magma residence times of basalt-hosted sapphires. Lithos 302:447–454

Baldwin L, Tomaschek F, Ballhaus C, Gerdes A, Fonseca R, Wirth R, Geisler T, Nagel T (2017) Petrogenesis of alkaline basalt-hosted sapphire megacrysts. Petrological and geochemical investigations of in situ sapphire occurrences from the Siebengebirge Volcanic Field, Germany. Contrib Mineral Petrol 172:1–27

Berndt J, Holtz F, Koepke J (2001) Experimental constraints on storage conditions in the chemically zoned phonolitic magma chamber of the Laacher See volcano. Contrib Mineral Petrol 140(4):469–486

Coenraads RR, Sutherland FL, Kinny PD (1990) The origin of sapphires: U-Pb dating of zircon inclusions sheds new light. Mineral Mag 54(374):113–122

Denis CM, Demouchy S, Shaw CS (2013) Evidence of dehydration in peridotites from Eifel Volcanic Field and estimates of the rate of magma ascent. J Volcanol Geotherm Res 258:85–99

Duda A, Schmincke H-U (1985) Polybaric differentiation of alkali basaltic magmas: evidence from green-core clinopyroxenes (Eifel, FRG). Contrib Mineral Petrol 91(4):340–353

Emmett JL, Scarratt K, McClure SF, Moses T, Douthit TR, Hughes R, Novak S, Shigley JE, Wang W, Bordelon O (2003) Beryllium diffusion of ruby and sapphire. Gems Gemol 39(2):84–135

Fekiacova Z, Mertz DF, Renne PR (2007) Geodynamic setting of the tertiary Hocheifel volcanism (Germany), part I: $^{40}Ar/^{39}Ar$ geochronology. Mantle plumes. Springer, Berlin, pp 185–206

Garcia-Castellanos D, Cloetingh S, Van Balen R (2000) Modelling the Middle Pleistocene uplift in the Ardennes-Rhenish Massif: thermo-mechanical weakening under the Eifel? Global Planet Change 27(1–4):39–52

Garlick GD, Epstein S (1967) Oxygen isotope ratios in coexisting minerals of regionally metamorphosed rocks. Geochim Cosmochim Acta 31(2):181–214

Giuliani G, Groat LA (2019) Geology of corundum and emerald gem deposits: a review. Gems Gemol 55:464–489

Giuliani G, Fallick A, Rakotondrazafy M, Ohnenstetter D, Andriamamonjy A, Ralantoarison T, Rakotosamizanany S, Razanatseheno M, Offant Y, Garnier V (2007) Oxygen isotope systematics of gem corundum deposits in Madagascar: relevance for their geological origin. Miner Deposita 42:251–270

Giuliani G, Fallick A, Ohnenstetter D, Pegere G (2009) Oxygen isotopes composition of sapphires from the French Massif Central: implications for the origin of gem corundum in basaltic fields. Miner Deposita 44:221–231

Giuliani G, Ohnenstetter D, Fallick A (2014) The geology and genesis of gem corundum deposits. In: Groat LA (ed) Geology of gem deposits. Mineralogical Association of Canada Short Course, Tucson, pp 29–112

Grapes RH (1986) Melting and thermal reconstitution of pelitic xenoliths, Wehr volcano, East Eifel, West Germany. J Petrol 27(2):343–396

Groat LA, Giuliani G, Stone-Sundberg J, Sun Z, Renfro ND, Palke AC (2019) A review of analytical methods used in geographic origin determination of gemstones. Gems Gemol 55(4):464–489

Gualda GA, Ghiorso MS, Lemons RV, Carley TL (2012) Rhyolite-MELTS: a modified calibration of MELTS optimized for silica-rich, fluid-bearing magmatic systems. J Petrol 53(5):875–890

Guo J, O'Reilly SY, Griffin WL (1996) Corundum from basaltic terrains: a mineral inclusion approach to the enigma. Contrib Mineral Petrol 122(4):368–386

Guo W, He H, Qiao L, Liu Z, Su F, Li J, Shi G, Zhu R (2022) Helium, neon and argon in alkaline basalt-related corundum megacrysts: implications for their origin and forming process. Geochim Cosmochim Acta 322:71–93

Harms E, Schmincke H-U (2000) Volatile composition of the phonolitic Laacher See magma (12,900 yr BP): implications for syneruptive degassing of S, F, Cl and H_2O. Contrib Mineral Petrol 138(1):84–98

Harms E, Gardner J, Schmincke H-U (2004) Phase equilibria of the Lower Laacher See Tephra (East Eifel, Germany): constraints on pre-eruptive storage conditions of a phonolitic magma reservoir. J Volcanol Geotherm Res 134(1–2):125–138

Hentschel G (1987) Die Mineralien der Eifelvulkane. 2. erweiterte Auflage. Christian Weise Verlag München

Holdaway M, Mukhopadhyay B (1993) A reevaluation of the stability relations of andalusite: thermochemical data and phase diagram for the aluminum silicates. Am Miner 78(3–4):298–315

Kato C, Moynier F, Foriel J, Teng F-Z, Puchtel IS (2017) The gallium isotopic composition of the bulk silicate Earth. Chem Geol 448:164–172

Kempton P, Harmon R, Stosch H-G, Hoefs J, Hawkesworth C (1988) Open-system O-isotope behaviour and trace element enrichment in the sub-Eifel mantle. Earth Planet Sci Lett 89(3–4):273–287

Kern OA, Koutsodendris A, Süfke F, Gutjahr M, Mächtle B, Pross J (2021) Persistent, multi-sourced lead contamination in Central Europe since the Bronze Age recorded in the Füramoos peat bog, Germany. Anthropocene 36:100310

Krylov DP, Evarestov RA (2018) Ab initio (DFT) calculations of corundum (α-Al_2O_3) oxygen isotope fractionation. Eur J Mineral 30(6):1063–1070

Levinson A, Cook F (1994) Gem corundum in alkali basalt: origin and occurrence. Gems Gemol 30(4):253–262

Lippolt HJ (1983) Distribution of volcanic activity in space and time. In: Fuchs K, von Gehlen K, Mälzer H, Murawski H, Semmel A (eds) Plateau uplift. Springer, Berlin, pp 112–120

Luvizotto GL, Zack T, Meyer H, Ludwig T, Triebold S, Kronz A, Muenker C, Stockli DF, Prowatke S, Klemme S (2009) Rutile crystals as potential trace element and isotope mineral standards for microanalysis. Chem Geol 261(3–4):346–369

Mertz DF, Löhnertz W, Nomade S, Pereira A, Prelević D, Renne PR (2015) Temporal–spatial evolution of low-SiO2 volcanism in the Pleistocene West Eifel volcanic field (West Germany) and relationship to upwelling asthenosphere. J Geodyn 88:59–79

Paces JB, Miller JD Jr (1993) Precise U-Pb ages of Duluth complex and related mafic intrusions, northeastern Minnesota: geochronological insights to physical, petrogenetic, paleomagnetic, and tectonomagmatic processes associated with the 1.1 Ga midcontinent rift system. J Geophys Res Solid Earth 98(B8):13997–14013

Palke AC, Renfro ND, Berg RB (2017) Melt inclusions in alluvial sapphires from Montana, USA: formation of sapphires as a restitic component of lower crustal melting? Lithos 278:43–53

Peucat J-J, Ruffault P, Fritsch E, Bouhnik-Le Coz M, Simonet C, Lasnier B (2007) Ga/Mg ratio as a new geochemical tool to differentiate magmatic from metamorphic blue sapphires. Lithos 98(1–4):261–274

Qin T, Wu F, Wu Z, Huang F (2016) First-principles calculations of equilibrium fractionation of O and Si isotopes in quartz, albite, anorthite, and zircon. Contrib Mineral Petrol 171:1–14

Rakotosamizanany S, Giuliani G, Ohnenstetter D, Rakotondrazafy AFM, Fallick AE, Paquette J-L, Tiepolo M (2014) Chemical and oxygen isotopic compositions, age and origin of gem corundums in Madagascar alkali basalts. J Afr Earth Sci 94:156–170

Reinig F, Wacker L, Jöris O, Oppenheimer C, Guidobaldi G, Nievergelt D, Adolphi F, Cherubini P, Engels S, Esper J (2021) Precise date for the Laacher See eruption synchronizes the Younger Dryas. Nature 595(7865):66–69

Riley TR, Bailey DK, Lloyd FE (1996) Extrusive carbonatite from the quaternary Rockeskyll complex, West Eifel, Germany. Canad Mineral 34(2):389–401

Rout SS, Wörner G (2020) Constraints on the pre-eruptive magmatic history of the Quaternary Laacher See volcano (Germany). Contrib Mineral Petrol 175(8):1–22

Schmidt S, Hertwig A, Schmitt AK, Cionoiu K, McKeegan KD, Bindeman I, Di Rocco T, Pack A (2024) A corundum reference material for oxygen isotope analysis by secondary ionization mass spectrometry. J Anal at Spectrom 39:439–446

Schmincke H-U (2007) The quaternary volcanic fields of the east and west Eifel (Germany). Mantle plumes. Springer, Berlin, pp 241–322

Schmitt AK, Zack T (2012) High-sensitivity U-Pb rutile dating by secondary ion mass spectrometry (SIMS) with an O_2^+ primary beam. Chem Geol 332:65–73

Schmitt AK, Wetzel F, Cooper KM, Zou H, Wörner G (2010) Magmatic longevity of Laacher See Volcano (Eifel, Germany) indicated by U-Th dating of intrusive carbonatites. J Petrol 51(5):1053–1085

Schmitt AK, Klitzke M, Gerdes A, Schäfer C (2017) Zircon Hafnium-Oxygen isotope and trace element petrochronology of intra-plate volcanic rocks from the Eifel (Germany) and implications for mantle versus crustal origins of zircon megacrysts. J Petrol 58(9):1841–1870

Schmitt AK, Klügel A, Böddeker S, Gothieu M, Gerdes A (2023a) Depth and timing of magma evolution underneath the Emmelberg scoria cone in the West Eifel Volcanic Field. N Jb Mineral Abh 198(2):101–118

Schmitt FH, Schmitt AK, Gerdes A, Harvey JC (2023b) Magma accumulation underneath Laacher See volcano from detrital zircon in modern streams. J Geol Soc Lond 180(1):jgs2022-2064

Seifert W, Rhede D, Förster H-J, Naumann R, Thomas R, Ulrych J (2014) Macrocrystic corundum and Fe–Ti oxide minerals entrained in alkali basalts from the Eger (Ohře) Rift: Mg−Fe^{3+}-rich ilmenite as tracer of an oxidized upper mantle. Mineral Petrol 108:645–662

Shaw CS, Eyzaguirre J, Fryer B, Gagnon J (2005) Regional variations in the mineralogy of metasomatic assemblages in mantle xenoliths from the West Eifel Volcanic Field, Germany. J Petrol 46(5):945–972

Shaw CS, Woodland AB, Hopp J, Trenholm ND (2010) Structure and evolution of the Rockeskyllerkopf Volcanic Complex, West Eifel Volcanic Field, Germany. Bull Volcanol 72:971–990

Simonet C, Fritsch E, Lasnier B (2008) A classification of gem corundum deposits aimed towards gem exploration. Ore Geol Rev 34(1–2):127–133

Sorokina ES, Rösel D, Häger T, Mertz-Kraus R, Saul JM (2017) LA-ICP-MS U-Pb dating of rutile inclusions within corundum (ruby and sapphire): new constraints on the formation of corundum deposits along the Mozambique belt. Miner Deposita 52:641–649

Sorokina ES, Botcharnikov RE, Kostitsyn YA, Rösel D, Häger T, Rassomakhin MA, Kononkova NN, Somsikova AV, Berndt J, Ludwig T (2021) Sapphire-bearing magmatic rocks trace the boundary between paleo-continents: a case study of Ilmenogorsky alkaline complex, Uralian collision zone of Russia. Gondwana Res 92:239–252

Stone-Sundberg J, Thomas T, Sun Z, Guan Y, Cole Z, Equall R, Emmett JL (2017) Accurate reporting of key trace elements in ruby and sapphire using matrix-matched standards. Gems Gemol 53:438–451

Stone-Sundberg JL, Guan Y, Sun Z, Ardon T (2021) Accurate trace element reporting in corundum: development of secondary ion mass spectrometry relative sensitivity factors. Geostand Geoanal Res 45(1):207–221

Sun Y, Schmitt AK (2019) ^{238}U/^{230}Th disequilibrium dating and trace element geochemistry of perovskite from late Quaternary alkali mafic rocks of the West Eifel Volcanic Field (Germany). Eur J Mineral 31(5–6):875–887

Sutherland F, Hoskin PW, Fanning CM, Coenraads RR (1998) Models of corundum origin from alkali basaltic terrains: a reappraisal. Contrib Mineral Petrol 133:356–372

Sutherland FL, Giuliani G, Fallick A, Garland M, Webb G (2009a) Sapphire-ruby characteristics, west Pailin, Cambodia: clues to their origin based on trace element and O isotope analysis. Aust Gemmol 23(9):373–432

Sutherland FL, Zaw K, Meffre S, Giuliani G, Fallick AE, Graham IT, Webb GB (2009b) Gem-corundum megacrysts from east Australian basalt fields: trace elements, oxygen isotopes and origins. Aust J Earth Sci 56(7):1003–1022

Sutherland FL, Coenraads RR, Abduriyim A, Meffre S, Hoskin P, Giuliani G, Beattie R, Wuhrer R, Sutherland G (2015) Corundum (sapphire) and zircon relationships, Lava Plains gem fields, NE Australia: integrated mineralogy, geochemistry, age determination, genesis and geographical typing. Mineral Mag 79(3):545–581

Sutherland FL, Graham IT, Harris SJ, Coldham T, Powell W, Belousova EA, Martin L (2017) Unusual ruby–sapphire transition in alluvial megacrysts, Cenozoic basaltic gem field, New England, New South Wales, Australia. Lithos 278:347–360

Turnier RB, Katzir Y, Kitajima K, Orland IJ, Spicuzza MJ, Valley JW (2020) Calibration of oxygen isotope fractionation and calcite-corundum thermometry in emery at Naxos, Greece. J Metamorph Geol 38(1):53–70

Uher P, Giuliani G, Szakall S, Fallick A, Strunga V, Vaculovič T, Ozdín D, Gregáňová M (2012) Sapphires related to alkali basalts from the Cerová Highlands, Western Carpathians (southern Slovakia): composition and origin. Geol Carpath 63(1):71–82

Upton B, Hinton R, Aspen P, Finch A, Valley J (1999) Megacrysts and associated xenoliths: evidence for migration of geochemically enriched melts in the upper mantle beneath Scotland. J Petrol 40(6):935–956

Upton B, Finch A, Słaby E (2009) Megacrysts and salic xenoliths in Scottish alkali basalts: derivatives of deep crustal intrusions and small-melt fractions from the upper mantle. Mineral Mag 73(6):943–956

Van den Bogaard P, Schmincke H (1990) Die Entwicklungsgeschichte des Mittelrheinraumes und die Eruptionsgeschichte des Osteifel-Vulkanfeldes. In: Schirmer W (ed) Rheingeschichte zwischen Mosel und Maas, Deuqua-Führer 1. Deutsche Quartärvereinigung, Hannover, pp 166–190

Van den Bogaard P, Hall CM, Schmincke HU, York D (1987) ^{40}Ar/^{39}Ar laser dating of single grains: ages of Quaternary tephra from the East Eifel Volcanic Field, FRG. Geophys Res Lett 14(12):1211–1214

Wagner GA, Storzer D (1970) Die Interpretation von Spaltspurenaltern (fission track ages) am Beispiel von natürlichen Gläsern, Apatiten Und Zirkonen. Eclogae Geol Helv 63(1):335–344

Wilson M, Downes H (2006) Tertiary-Quaternary intra-plate magmatism in Europe and its relationship to mantle dynamics. Geol Soc Lond Memoirs 32(1):147–166

Wong J, Verdel C (2018) Tectonic environments of sapphire and ruby revealed by a global oxygen isotope compilation. Int Geol Rev 60(2):188–195

Wong J, Verdel C, Allen CM (2017) Trace-element compositions of sapphire and ruby from the eastern Australian gemstone belt. Mineral Mag 81(6):1551–1576

Wörner G, Fricke A (1984) Fluid inclusions in corundum from a contact metamorphic xenolith of the Quaternary Wehr volcano (East Eifel, Germany). N Jb Mineral Mh 1984:39–47

Wörner G, Schmincke H-U (1984) Mineralogical and chemical zonation of the Laacher See tephra sequence (East Eifel, W. Germany). J Petrol 25(4):805–835

Wörner G, Schmincke H-U, Schreyer W (1982) Crustal xenoliths from the Quaternary Wehr volcano (East Eifel). N Jb Mineral Abh 144:29–55

Wörner G, Staudigel H, Zindler A (1985) Isotopic constraints on open system evolution of the Laacher See magma chamber (Eifel, West Germany). Earth Planet Sci Lett 75(1):37–49

Wörner G, Harmon R, Hoefs J (1987) Stable isotope relations in an open magma system, Laacher See, Eifel (FRG). Contrib Mineral Petrol 95:343–349

Wörner G, Viereck L, Plaumann S, Pucher R, van den Bogaard P, Schmincke H (1988) The Quaternary Wehr volcano: a multiphase evolved eruption center in the east Eifel volcanic field (FRG). N Jb Miner Abh 159(1):73–99

Xu X-S, Chen X-M, Griffin WL, O'Reilly SY, Zhang X-S, Chen L-H (2021) Immiscible-melt inclusions in corundum megacrysts: microanalyses and geological implications. Am Miner 106(4):559–569

Zhao Z-F, Zheng Y-F (2003) Calculation of oxygen isotope fractionation in magmatic rocks. Chem Geol 193(1–2):59–80

Zheng Y-F, Fu B (1998) Estimation of oxygen diffusivity from anion porosity in minerals. Geochem J 32(2):71–89